

Design and Optimization of Feedforward-PID Integrated Controller for Pre-Injection Numerical Control Air-Powered Engine

Zhao Caihong^{1,*}, Chen Shian² and Zhang Shijin²

¹Nanhang Jincheng College, Nanjing 211156, P.R. China

²School of Automotive and Traffic Engineering, Jiangsu University, Zhenjiang, P.R. China

Abstract: A feedforward-PID integrated controller is developed and optimized for the pre-injection numerical control (NC) air-powered engine (PINCAPE) to track the expected speed quickly and accurately. The proposed integrated controller comprises two parts, namely a feedforward controller and a PID one. According to the real-time workload and the expected speed, the feedforward controller uses a numerical fitting function to determine the main part of the supply air pressure to obtain good stable accuracy. The function is developed with the output of the supply air pressure, and the inputs of the engine speed and the output power, which are based on the different steady-state operations of the engine. To improve the engine response performance, the PID controller gives the fine-tuning of the supply air pressure with the input of the difference between the expected speed and the real-time speed. The parameters of the PID controller are optimized according to the genetic algorithm, with an objective function that minimizes the mean square of the speed error. The results show that the optimized feedforward-PID integrated controller shortens the response time of the PINCAPE by more than 47% and 64.5% under varied set point speed and engine load variations respectively, compared with the single feedforward controller. Furthermore, the response steady state error of the feedforward-PID integrated controller is less than 1%, which perfectly satisfies the control specification.

Keywords: Air-powered engine, feedforward-PID integrated controller, genetic algorithm, NC, pre-injection.

1. INTRODUCTION

Two major problems that are facing our world today are the environment pollution and the energy crisis. The environment pollution and the energy crisis are due to more vehicles, most of which are powered by internal combustion engines using fossil fuel [1, 2].

The air-powered engine can give renewable power and zero emission because that is driven by compressed air which can be produced from solar, wind energy, water energy and so on [3-7]. Therefore the air-powered engine becomes more popular and is regarded as one of the ideal power sources for future vehicles.

Although there is an air-powered swash plate engine reported [8], most of air-powered engines resemble to common internal combustion engines. The air-powered engine at least has a cylinder, a piston, a crank, a valve train system, and so on. During the air-powered engine operation, there are working stroke and exhaust stroke. With the help of the valve train system, the working stroke puts compressed air into the cylinder and expands. The high pressure air expansion gives power by the piston and the crank motion. Exhaust stroke gets rid of expanded pressure air from the cylinder.

Air intake and exhaust of the air-powered engine are through by intake and exhaust valves of the valve train system. Because intake air pressure is much larger than the atmospheric pressure, there are difficulties in seals of the valve train system. To settle down these difficulties, a pre-injection numerical control air-powered engine (PINCAPE) is firstly given by the authors [9].

Fig. (1) shows the working scheme of the PINCAPE. The PINCAPE is at least made of a third high-pressure air tank, a pre-injection cylinder, solenoid valves, sensors and an ontology engine, without a valve timing mechanism. The pre-injection cylinder and the controlled solenoid valves are set to perform the functions of the valve train system, so these seal matters in the valve train system are expected to be settled down and the energy (mass of compressed air) to the PINCAPE can be precisely provided according to its power requirement.

Chen *et al.* presented respective influences of intake advance angle, basal of intake sustain angle, exhaust advance angle and exhaust delay angle on the energy conversion efficiency and the output torque of the air-powered engine [10]. However, their model was not dynamic since it is based on the angular coordinate without time variation. The paper developed a non-linear model of the PINCAPE that fully displayed inner thermodynamic characteristics.

*Address correspondence to this author at the School of Mechanical Engineering, Nanhang Jincheng College, Nanjing, Jiangsu, 211156, P.R. China; Tel: +86 25 87190150; E-mail: 7766733@qq.com

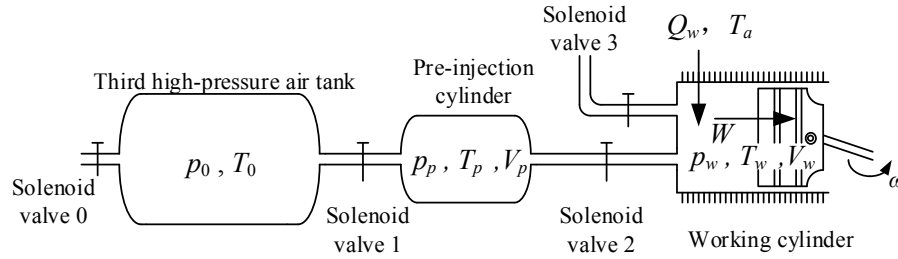


Fig. (1). working scheme of PINCAPE.

The engine with good performances should respond quickly and precisely to the speed operation. The speed control method of the existing air-powered engine with a valve train system is similar to the common internal combustion engine. The current method uses a governor to change the effective flow area of air intake to the cylinder to control the output power (or torque). Although the mechanical governor replaced by an electronic governor, the control accuracy and energy efficiency is not ideal [11]. The reason is that the control procedure is synchronous with the air intake process.

The PINCAPE has a characteristic that the amount of compressed air intake is prepared in advance of compressed air intake of the working cylinder. Hence, higher control accuracy and higher energy efficiency is expected to reach when a good speed control controller is adopted for the PINCAPE.

To improve response rate and control accuracy to the expected speed of the speed operation, the paper proposes and optimizes a feedforward-PID integrated controller for PINCAPE. The feedforward-PID integrated controller consists of a feedforward controller and a PID controller. The feedforward controller plays the role to decide the main supply pressure of the pre-injection cylinder to obtain good stable accuracy. The PID controller plays the role to decide the fine tuning supply pressure to fasten the engine's response rate. To achieve a good control effect, the PID control parameters are optimized according to the genetic algorithm (GA) [12, 13].

2. THERMO-DYNAMICS MODEL OF PINCAPE

As shown in Fig. (1), during the working stroke, the solenoid valve 2 opens, after compressed air flows into the working cylinder from the pre-injection cylinder to drive the piston and the crank, the ontology engine supplies power by the flywheel.

There are those basic hypotheses [10]:

- (1) The high-pressure air is ideal gas.
- (2) p_0 and T_0 are constants which are the absolute pressure and the absolute temperature in the third high-pressure air tank respectively.
- (3) Equal pressure and equal temperature are throughout the pre-injection cylinder and the working cylinder.

Control strategies of the solenoid valves 1, 2 and 3 are arranged as follows.

- (1) The solenoid valve 1 opens at the start of the exhaust stroke and closes when the expected control pressure of

the pre-injection cylinder p_{pec} is reached.

- (2) The solenoid valve 2 just opens during the working stroke.
- (3) The solenoid valve 3 opens during the exhaust stroke and when the absolute pressure in the working cylinder p_w is larger than the atmospheric pressure p_a .

K_1 , K_2 and K_3 , the switching values of the solenoid valves 1, 2 and 3, are expressed as.

$$\begin{cases} K_1 = \text{hardlim}(p_{pec} - p_p) \times (1 - K_2) \\ K_2 = \text{hardlim}[\sin(\omega t)] \\ K_3 = \text{hardlim}(p_w - p_a) \times (1 - K_2) \end{cases} \quad (1)$$

Where the $\text{hardlim}(\cdot)$ is the hard-limit transfer function, ω is the engine speed with the unit of rad/s, t is time.

2.1. Thermo-Flow Rate Model of Pre-Injection Cylinder

During intake and exhaust of the pre-injection cylinder, there are thermodynamics equations as follows [14].

$$\frac{dU_p}{dt} = K_1 \times \frac{dH_1}{dt} - K_2 \times \frac{dH_2}{dt} \quad (2)$$

$$\frac{dU_p}{dt} = \frac{d(m_p u_p)}{dt} = \frac{d(m_p c_p T_p)}{dt} \quad (3)$$

$$p_p V_p = m_p R T_p \quad (4)$$

$$\frac{dH_1}{dt} = h_0 \frac{dm_1}{dt} = c_p T_0 \frac{dm_1}{dt} = c_p T_0 q_1 \quad (5)$$

$$\frac{dH_2}{dt} = h_p \frac{dm_2}{dt} = c_p T_p \frac{dm_2}{dt} = c_p T_p q_2 \quad (6)$$

Where U_p , H_1 and H_2 are the internal energy in the pre-injection cylinder, the enthalpy flowing through the solenoid valve 1 and the enthalpy flowing through the solenoid valve 2 respectively; c_p and c_v are the specific heat capacity at constant pressure and the specific heat capacity at constant volume respectively; m_p is the air mass within the pre-injection cylinder; m_1 and m_2 are the air mass flowing through the solenoid valve 1 and the air mass flowing through the solenoid valve 2 respectively; h_p and u_p are the specific enthalpy and the specific internal energy of the air in the pre-injection cylinder respectively; h_0 is the specific enthalpy of the air in the third high-pressure air tank; R is the gas constant; q_1 and q_2 are the air flow through the solenoid valve 1 and the air flow through the solenoid valve 2 respectively.

The pressure-flow equations of during intake and exhaust of the pre-injection cylinder are written as follows.

$$\begin{cases} q_1 = A_1 p_0 \sqrt{\frac{2k}{k-1} \frac{1}{RT_0}} \phi_1(\sigma_1), & \sigma_1 = \frac{p_p}{p_0} \\ q_2 = A_2 p_p \sqrt{\frac{2k}{k-1} \frac{1}{RT_p}} \phi_2(\sigma_2), & \sigma_2 = \frac{p_w}{p_p} \end{cases} \quad (7)$$

Where A_1 and A_2 are the effective flowing area of the solenoid valve 1 and the effective flowing area of the solenoid valve 2 respectively; k is the specific heat ratio; ϕ_1 and ϕ_2 are the stream functions associated with the pressure different through the solenoid valves 1 and 2 respectively.

ϕ_1 and ϕ_2 are written as follows [10].

$$\phi_i(\sigma_i) = \begin{cases} \sqrt{\sigma_i^{\frac{2}{k}} - \sigma_i^{\frac{k+1}{k}}}, & \sigma_i > 0.528 \\ \sqrt{\left(\frac{2}{k+1}\right)^{\frac{2}{k-1}} - \left(\frac{2}{k+1}\right)^{\frac{k+1}{k-1}}}, & \sigma_i \leq 0.528 \end{cases} \quad (i=1,2) \quad (8)$$

Take Equations (3), (4), (5) and (6) into Equation (2), $\frac{dp_p}{dt}$ can be expressed as following.

$$\frac{dp_p}{dt} = \frac{kRT_0}{V_p} (K_1 \times q_1) - \frac{kRT_p}{V_p} (K_2 \times q_2) \quad (9)$$

2.2. Thermo-Flow Rate Model of Working Cylinder

During the working stroke and the exhaust stroke of the working cylinder, there are thermodynamics equations as follows.

$$\frac{dQ_w}{dt} = \frac{dU_w}{dt} - K_2 \times \frac{dH_2}{dt} + K_3 \times \frac{dH_3}{dt} + \frac{dW}{dt} \quad (10)$$

$$\frac{dU_w}{dt} = \frac{d(m_w u_w)}{dt} = \frac{d(m_w c_v T_w)}{dt} \quad (11)$$

$$p_w V_w = m_w RT_w \quad (12)$$

$$\frac{dQ_w}{dt} = a_g A_g (T_a - T_w) \quad (13)$$

$$\frac{dH_3}{dt} = h_w dm_3 = c_p T_w dm_3 = c_p T_w q_3 \quad (14)$$

$$\frac{dW}{dt} = p_w \frac{dV_w}{dt} \quad (15)$$

Where Q_w , U_w , H_3 and W are the heat exchange between the air within the working cylinder and the environment, the internal energy within the working cylinder, the enthalpy flowing through the solenoid valve 3 and the power from compressed air within the working cylinder to the piston respectively; m_w is the air mass within the working cylinder; m_3 is the air mass flowing through the solenoid valve 3; h_w and u_w are the specific enthalpy and the specific internal en-

ergy of the air within the working cylinder respectively; q_3 is the air flow through the solenoid valve3; a_g is the heat exchange coefficient between the air within the working cylinder and the environment [15]; A_g is the heat exchange area; T_a and T_w are the atmospheric temperature and the air temperature within the working cylinder respectively; V_w is the working volume of the working cylinder.

$$a_g = 1.28 \sqrt[3]{\omega} \sqrt{\frac{p_w}{10^5} T_w} = 0.004 \sqrt[3]{\omega} \sqrt{p_w T_w} \quad (16)$$

$$q_3 = A_3 p_w \sqrt{\frac{2k}{k-1} \frac{1}{RT_w}} \phi_3(\sigma_3), \quad \sigma_3 = \frac{p_a}{p_w} \quad (17)$$

$$\phi_3(\sigma_3) = \begin{cases} \sqrt{\sigma_3^{\frac{2}{k}} - \sigma_3^{\frac{k+1}{k}}} & \sigma_3 > 0.528 \\ \sqrt{\left(\frac{2}{k+1}\right)^{\frac{2}{k-1}} - \left(\frac{2}{k+1}\right)^{\frac{k+1}{k-1}}} & \sigma_3 \leq 0.528 \end{cases} \quad (18)$$

V_w , A_g , $\frac{dV_w}{dt}$ and a_g are written as follows [16, 17].

$$V_w = V_{w0} + \frac{V_h}{2} (1 - \cos \varphi + \frac{\lambda}{2} \sin^2 \varphi) \quad (19)$$

$$V_h = 2rS \quad (20)$$

$$S = \frac{\pi D^2}{2} \quad (21)$$

$$A_g = 2S + \pi Dr (1 - \cos \varphi + \frac{\lambda \sin^2 \varphi}{2}) \quad (22)$$

$$\frac{dV_w}{dt} = \frac{\omega V_h}{2} (\sin \varphi + \frac{\lambda}{2} \sin 2\varphi) \quad (23)$$

$$\omega = \dot{\varphi} \quad (24)$$

Where A_3 is the effective flowing area of the solenoid valve 3; V_{w0} is the minimum of V_w ; V_h is the displacement of the working cylinder; φ is the engine displacement; r is the radius of the crank; λ is the connecting rod ratio; D is the diameter of the working cylinder; S is the cross-sectional area of the working cylinder respectively.

Taking Equations (11), (12), (13), (14), (15) and (19) into Equation (10), $\frac{dp_w}{dt}$ can be expressed as following.

$$\begin{aligned} \frac{dp_w}{dt} = & \frac{Ra_g A_g}{c_v V_w} (T_a - T_w) + \frac{kRT_p}{V_w} (K_2 \times q_2) \\ & - \frac{kRT_w}{V_w} (K_3 \times q_3) - \frac{kp_w}{V_w} \frac{dV_w}{dt} \end{aligned} \quad (25)$$

2.3. Dynamics Model of Ontology Engine

When kinematics analyses and dynamics analyses on the ontology engine are carried out, following equations are obtained.

$$M_p = r[(p_w - p_a)S - m_i r \omega^2 (\cos \varphi + \lambda \cos 2\varphi)] \times (\sin \varphi + \frac{\lambda \sin 2\varphi}{2\sqrt{1 - \lambda^2 \sin^2 \varphi}}) \quad (26)$$

$$M_p - M_l = I_f \ddot{\varphi} \quad (27)$$

Where M_p and M_l are the torque output of the piston and the resisting torque of the engine load respectively; I_f is the moment of inertia on the flywheel; m_i is the reciprocating mass in the working cylinder.

M_l is given as follows [18].

$$\begin{cases} M_l = M_{l0} \text{sign}(\omega) + k_l \omega, & \omega \neq 0 \\ -M_{l0} \leq M_l \leq M_{l0}, & \omega = 0 \end{cases} \quad (28)$$

Where k_l is the linear resisting torque coefficient; M_{l0} is the coulomb damping of the engine.

3. DESIGN OF FEEDFORWARD-PID INTEGRATED CONTROLLER FOR PINCAPE

The design and optimization of the feedforward-PID integrated controller for the PINCAPE are employed by numerical simulations.

The PINCAPE is reformed from an S195 engine, the parameter values in simulations are listed in Table 1.

Table 1. Parameters in simulation.

Parameter	Value	Parameter	Value
A_1 / m^2	7.854×10^{-5}	k	1.4
A_2 / m^2	7.854×10^{-5}	$c_v / \text{J} \cdot \text{kg}^{-1} \cdot \text{K}^{-1}$	717.9
A_3 / m^2	1.5708×10^{-4}	$c_p / \text{J} \cdot \text{kg}^{-1} \cdot \text{K}^{-1}$	1005
D / m	0.095	$R / \text{J} \cdot \text{kg}^{-1} \cdot \text{K}^{-1}$	287.1
r / m	0.0575	p_0 / Pa	10^7
λ	0.2738	p_a / Pa	1.01×10^5
V_p / m^3	1.3586×10^{-4}	p_{p0} / Pa	2×10^6
V_{w0} / m^3	2×10^{-5}	p_{w0} / Pa	1.01×10^5
m_i / kg	2.325	T_a / K	300
$M_{l0} / \text{N} \cdot \text{m}$	0.2	T_{p0} / K	300
$I_f / \text{kg} \cdot \text{m}^2$	0.253	T_{w0} / K	300
$\omega_0 / \text{rad} \cdot \text{s}^{-1}$	0.2094		

p_{p0} , p_{w0} , T_{p0} , T_{w0} and ω_0 are the initial values of p_p , p_w , T_p , T_w and ω respectively.

When M_l is set as constant ($k_l = 0.25 \text{ N} \cdot \text{m} \cdot \text{s} \cdot \text{rad}^{-1}$), p_{pec} is changed among 0.8 MPa, 1.6 MPa and 2.4 MPa, the n_r - t curves of the PINCAPE are given in Fig. (2). Here, n_r is the real-time speed of the engine.

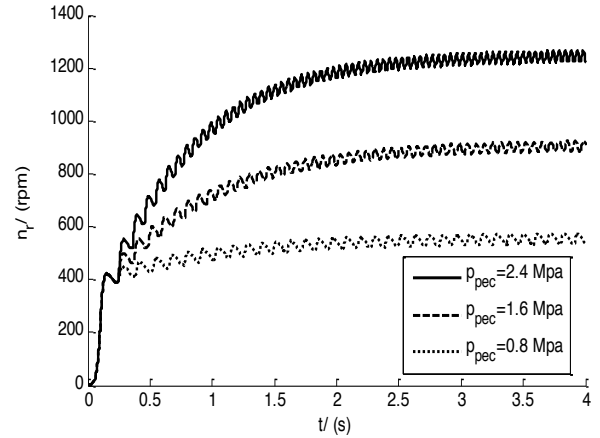


Fig. (2). n_r - t curve of PINCAPE.

Fig. (2) shows that the start-up of the PINCAPE is good because it is into working stably less than 1.5 seconds after start. The engine speed increases in air stroke and decreases in exhaust stroke when the engine is stably working and similar to common internal combustion engines. Hence, the model of PINCAPE developed in this paper is dynamic and feasible.

The vehicle equipped with a PINCAPE needs to track the expected speed quickly and accurately. A slow speed response of the engine will cause a bad vehicle dynamic performance and bring large engine speed fluctuations which lead to bad comforts. To satisfy this objective, an integrated controller with feedforward- PID approach is introduced. In a PINCAPE speed control system, the engine speed is controlled by p_{pec} , the expected control pressure of the pre-injection cylinder [9]. The control input is calculated from the real-time engine load k_l , the expected speed n_{igt} and the real-time engine speed n_r . k_l and n_r can be measured by the crank sensors. Fig. (3) shows the block diagram of the feedforward-PID integrated controller.

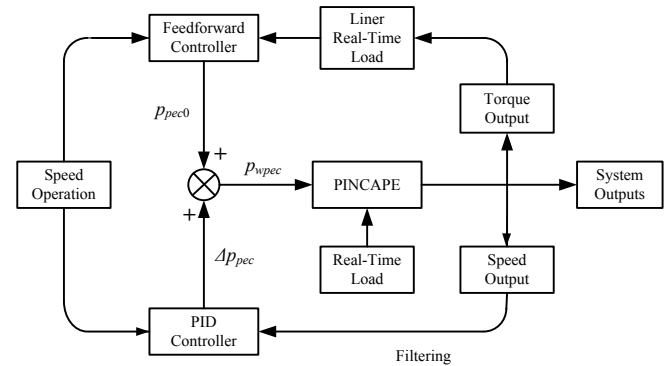


Fig. (3). block diagram of feedforward-PID integrated controller.

The feedforward-PID integrated controller gives p_{wpec} which is the whole control pressure. p_{wpec} is set to equal the sum of the main supply pressure of the pre-injection cylinder p_{pec0} and the fine tuning supply pressure of the pre-injection cylinder $\Delta p_{pec} \cdot p_{pec0}$ and Δp_{pec} are given by a feedforward loop and a PID loop respectively.

3.1. Feedforward Controller

The feedforward controller gives p_{pec0} by using $p_{pec0} = f(n_{igt}, p_{igt})$, where the control function of p_{pec0} is expressed by n_{igt} and p_{igt} . p_{igt} is the output power of the engine under k_l and n_{igt} . p_{igt} is written as follows.

$$p_{igt} = k_l \left(\frac{\pi n_{igt}}{30} \right)^2 / 1000 \tag{29}$$

$$k_l = \frac{M_{pr} - M_{lr} - I_f \dot{\omega}}{\omega + 0.001} \tag{30}$$

Where M_{pr} is the measured value by the torque sensor on the crank, and M_{lr} is the value of idling operation. To obtain stable p_{igt} , k_l is replaced by k_{lr} , which is filtered value of k_l by using an Analog Filter design in Simulink [19, 20].

$p_{pec0} = f(n_{igt}, p_{igt})$ is extremely important to the feedforward controller. In order to obtain an accurate p_{pec0} , the function is established through numerical fitting method according to data of p_{spec} , n_s and p_s , which are obtained in many different steady state engine operations. The data needed in numerical fitting are shown in **Accessory 1**.

p_{spec} is expressed as following.

$$p_{spec} = a_{11}n_s + a_{12}p_s + a_{21}n_s^2 + a_{22}n_s p_s + a_{23}p_s^2 + L a_{j1}n_s^j + L a_{j(j+1)}p_s^j \quad (j \geq 3) \tag{31}$$

Where $a_{11} \sim a_{j(j+1)}$ are fitting parameters respectively. δ , which is the residual between p_{specF} and p_{spec} , is introduced by [21].

$$\delta = \frac{\left[\sum_{i=1}^h |p_{specFi} - p_{speci}| \right] / h}{\left[\sum_{i=1}^h |p_{speci}| \right] / h} \tag{32}$$

Where h is the measuring point number, p_{specF} is the fitted value of p_{spec} .

When j equals to 2, 3 and 4 respectively, the corresponding values of δ are listed in Table 2.

Table 2. Residuals fitted of feedforward control function

	j		
	2	3	4
δ	0.0870	0.0133	0.0153

Table 2 shows that δ is minimal when j equals to 3. Therefore, the manipulated variables of the feedforward control loop based on steady state function Equation (31) can be calculated by

$$p_{pec0} = f(n_{igt}, p_{igt}) = 0.2778n_{igt} + 2.9189p_{igt} - 0.13n_{igt}^2 - 5.3434n_{igt}p_{igt} - 0.0994p_{igt}^2 - 0.0436n_{igt}^3 + 3.3452n_{igt}^2p_{igt} + 0.4572n_{igt}p_{igt}^2 - 0.0064p_{igt}^3 \tag{33}$$

3.2. PID Controller

A standard PID controller, which is made of the proportional, the integral and derivative [22], is written as follows.

$$\Delta p_{pec} = k_p e + k_i \int_0^t e dt + k_d \frac{de}{dt} \tag{34}$$

$$e = n_{igt} - n \tag{35}$$

Where Δp_{pec} is the fine tuning supply pressure to compensate the feedforward action to track the expected speed; k_p , k_i and k_d are the proportional, integral and derivative parameters respectively. In view that n_r is fluctuating even if the engine works stably. To ensure the PID controller works smoothly, n_r is replaced by n , which is the real-time mean value of n_r .

4. OPTIMIZED RESULTS AND COMPARISON

A speed operation has been applied for optimizing parameters of the designed feedforward-PID integrated controller which is that the initial engine speed was 0 rpm, in 0~15 s the expected speed is 900 rpm, in 15-30 s the expected speed is 1200 rpm, in 30-45 s the expected speed is 900 rpm, and k_l is 0.5 N·m·s·rad⁻¹.

We propose a determination method to minimize the function below.

$$J = \int_0^t e^2 dt \tag{36}$$

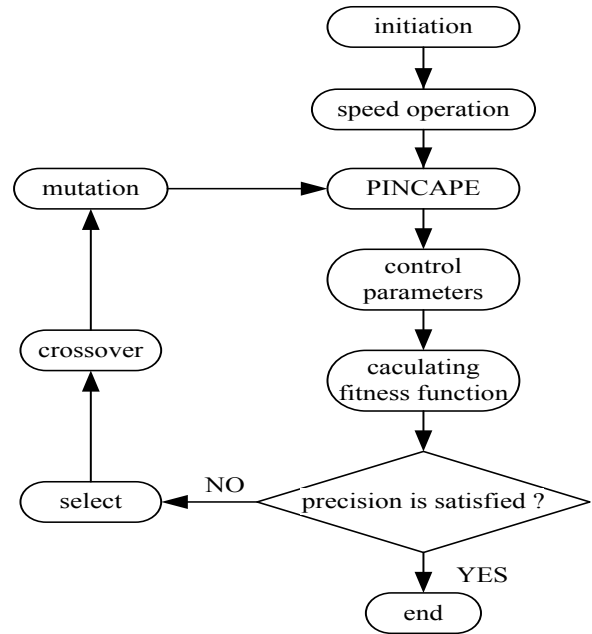


Fig. (4). Flow chart for optimizing the feedforward-PID integrated controller based on GA.

The genetic algorithm (GA) is a powerful search technique which has been applied to many practical problems. Hence, GA is chosen as the optimizing method for the feedforward-PID integrated controller [23]. During optimization procedure, GA iteratively manipulates populations of these

chromosomes using reproduction, crossover and mutation operations, and evaluates suitability of each solution using a fitness function. Here the optimization objective function J is taken as the fitness function. Chromosomes with a good fit are carried forward into the next generation and are subsequently used as the basis for generating new and improved solutions. The search procedure continues iteratively until the specified termination conditions have been satisfied. It is that the solution with desired fitness is satisfied for a specified number of generations. Flow chart for optimizing the feedforward-PID integrated controller based on GA is shown in Fig. (4).

The parameters for the GA-based optimizing procedure are selected as follows.

- 1) Maximum number of generation: 50;
- 2) Initial population size: 60;
- 3) Crossover probability: 0.9;
- 4) Mutation probability: 0.7;
- 5) Generation gap: 0.9;
- 6) $k_d \in [0, 50]$, $k_i \in [0, 50000]$ and $k_p \in [0, 3500]$.

Consequently, after 50 generations, $k_d=3.7$, $k_i=265.3$ and $k_p=2991.5$ are obtained, change of population optimal solution is shown in Fig. (5). The $n-t$ curves and $p_{wpec}-t$ curves are shown in Figs. (6, 7).

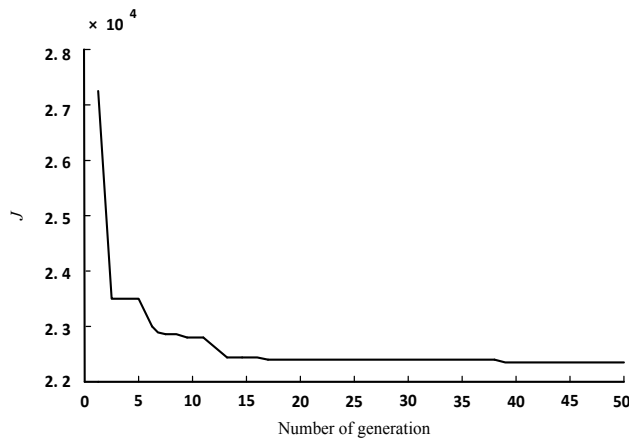


Fig. (5). Change of population optimal solution.

Fig. (6) shows the feedforward controller takes 2.42s from 0 rpm to 900 rpm, 1.6s from 900 rpm to 1200 rpm, and 1.3s from 1200 rpm to 900 rpm. The corresponding times of the feedforward-PID integrated controller are 0.8s, 0.49s, and 0.69s, respectively. Thus, the feedforward-PID integrated controller is faster than the feedforward controller. As shown in Fig. (7), the reason is that the PID controller plays useful roles to improve the control compensation performance. Fig. (6) shows that e is 1 rpm when the engine stably works at 900rpm and e is 8 rpm when the engine stably works at 1200rpm. Therefore, the feedforward-PID integrated controller has an ability of tracking the speed operation accurately.

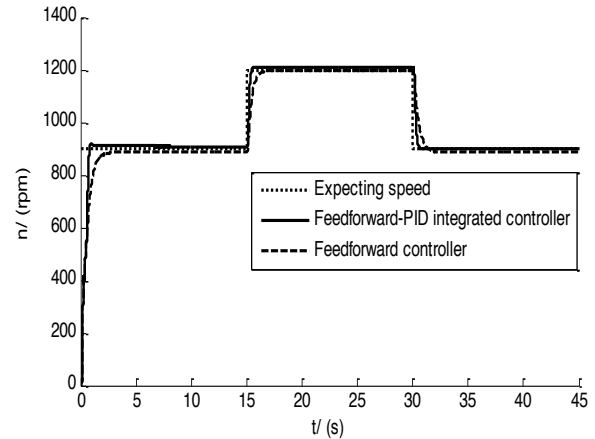


Fig. (6). $n-t$ curves when n_{tgt} varies.

To verify the efficacy of the feedforward-PID integrated controller, intermittent operations at load variations are simulated. The intermittent operations are that n_{tgt} is fixed to 900 rpm, the k_i was varied from $0.1 \text{ N}\cdot\text{m}\cdot\text{s}\cdot\text{rad}^{-1}$ to $1 \text{ N}\cdot\text{m}\cdot\text{s}\cdot\text{rad}^{-1}$ at the 15th second and from $1 \text{ N}\cdot\text{m}\cdot\text{s}\cdot\text{rad}^{-1}$ to $0.1 \text{ N}\cdot\text{m}\cdot\text{s}\cdot\text{rad}^{-1}$ at the 30th second. The k_i-t curve, $n-t$ curves and $p_{wpec}-t$ curves are shown in Figs. (8-10).

Fig. (9). shows when k_i varies, the feedforward controller takes 1.21s and 5.8s to stably reach 900 rpm. The corresponding times of the feedforward-PID integrated controller are 0.43s and 1.45s respectively. The reason is that the feedforward-PID integrated controller gives much bigger p_{wpec} when k_i increases and vice versa as shown in Fig. (10). Therefore, the feedforward-PID integrated controller has a good robustness.

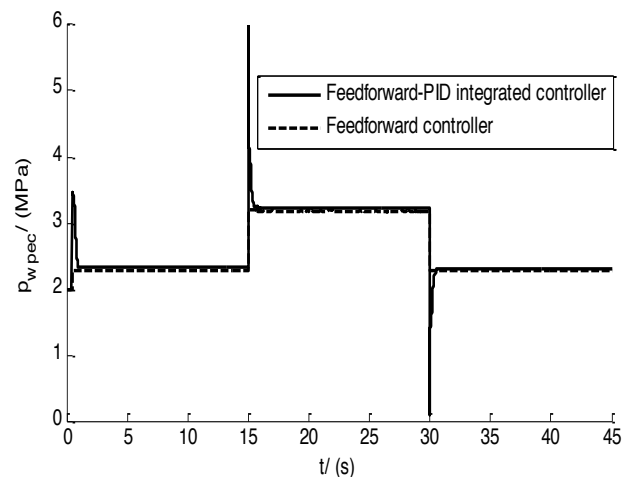


Fig. (7). $p_{wpec}-t$ curves when n_{tgt} varies.

CONCLUSION

Based on the thermo-dynamics model of PINCAPE, this paper designs a robust feedforward-PID integrated controller that includes a feedforward controller and a PID controller to implement the engine speed control. For the tracking, accuracy and robustness, we compare with the feedforward con-

troller used only and confirm the effectiveness of the proposed controller.

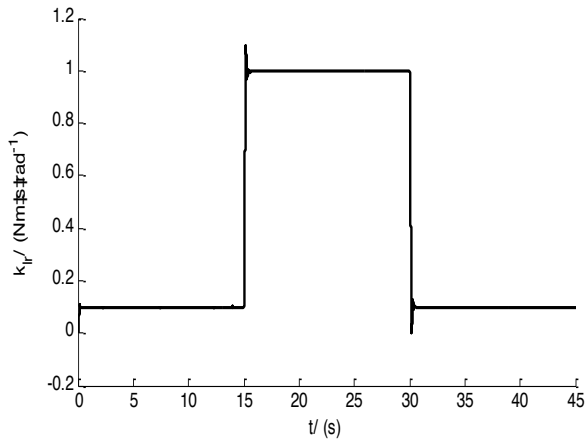


Fig. (8). k_{tr} - t curve.

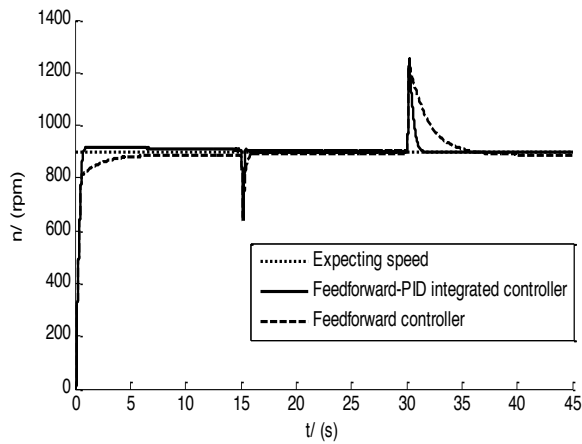


Fig. (9). n - t curves when k_i varies.

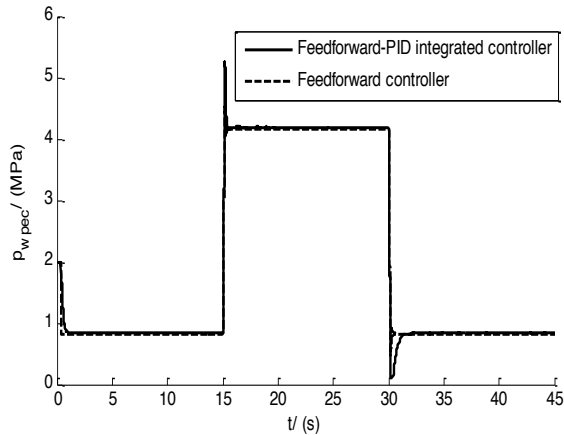


Fig. (10). p_{wpec} - t curves when k_i varies.

In the future we plan to perform experiments about a feedforward-PID integrated controller, not only verify this control method, but also offer a reference for using of control on PINCAPE.

ACCESSORY 1

All of data are recorded in Table 3

Table 3. n_s and p_s recorded in each p_{spec}

p_{spec} (MPa)	n_s (100r/min)	p_s (kW)	p_{spec} (MPa)	n_s (100r/min)	p_s (kW)
2	23.3	3.4	2	22.5	3.7
2	21.6	3.9	2	21.0	4.1
2	20.2	4.3	2	19.6	4.4
2	16.9	4.8	2	14.8	4.9
2	13.0	4.7	2	11.5	4.4
2	10.3	4.1	2	9.3	3.8
2	8.4	3.5	2	7.7	3.1
2	7.1	3.0	2	6.5	2.8
2	6.1	2.6	2	5.7	2.5
3	22.6	5.7	3	20.1	6.8
3	18.2	7.4	3	15.3	7.8
3	13.2	7.7	3	11.4	7.2
3	10.0	6.7	3	8.9	6.0
3	7.9	5.5	3	7.1	5.0
3	6.5	4.6	3	5.9	4.3
4	24.2	6.5	4	22.0	8.0
4	20.2	9.0	4	17.5	10.1
4	15.4	10.5	4	13.8	10.4
4	12.4	10.2	4	11.3	9.8
4	10.2	9.2	4	9.4	8.7
4	8.6	8.2	4	7.9	7.7
5	23.4	9.0	5	21.7	10.4
5	20.2	11.3	5	19.1	12.0
5	17.1	12.8	5	15.4	13.1
5	14.1	13.1	5	12.9	12.9
5	12.0	12.6	5	11.1	12.2
5	10.3	11.7	5	9.6	11.2
5	9.0	10.7	5	8.4	10.2
5	7.9	9.7	5	7.4	9.3
5	7.0	8.8	5	6.6	8.4
5	6.3	8.0	5	5.9	7.6

CONFLICT OF INTEREST

The authors confirm that this article content has no conflict of interest.

ACKNOWLEDGEMENTS

This research is financially supported by the National Natural Science Fund Project of China under the contract 50805066 and the Scientific Research Foundation for Talented Scholars of Jiangsu University under the contract 06jdg040.

REFERENCES

- [1] L.G. Liu, "Development and research of the automobile in the 21st century", *Chinese Journal of Automobile Research and Development*, no. 1, pp. 8-10, 2001.
- [2] Y. Z. Bian, "Automobile New Energy Technology", Beijing: People's Traffic Press, 2003.
- [3] J. Williams, C. Knowlen, A. T. Mattick and A. Hertzberg, "Quasi Isothermal Expansion Engines For Liquid Nitrogen Automotive Propulsion", SAE Paper, no. 972649, 1997.
- [4] H. Liu, Y. Chen and G.L. Tao, "Researches on characteristics and model of work process of compressed air powered engine", *Progress in Natural Science*, no. 14, pp. 319-324, 2004.
- [5] P.L. Chen, X.L. Yu and L. Liu, "Simulation and experimental study of electro-pneumatic valve used in air-powered engine", *Journal of Zhejiang University (Science A)*, no. 10, pp. 377-383, 2009.
- [6] H.G. Liu, B.B. Gu, F. Qiu and S.A. Chen, "Testing and Numerical Fitting of Cornering Stiffness of 7.50R20 14PR PW02Tire", *Tractor & Farm Transporter*, no. 36, pp. 63-65, 2009.
- [7] S.A. Chen, R He, S.L. Lu and M. Yao, "Modeling of air-powered engine based on time coordinate and optimal approach of gas distribution parameters", *Proceedings of the ASME International Design Engineering Technical Conference & Computers and Information in Engineering Conference, IDETC/CIE2010*, no. 4, pp. 219-227, 2010.
- [8] Y.Q. Lian, S.Z. Wang, S.J. Ma, Y.H. Chen and Z.J. Li, "Dynamic simulation of the air-powered swash plate engine", *Chinese Journal of Mechanical Engineering*, no. 44, pp. 243-248, 2008.
- [9] S.A. Chen, S.J. Zhang and R. He, "Operating properties of pre-injection NC air-powered engine", *Journal of Traffic and Transportation Engineering*, no. 1, pp. 35-41, 2011.
- [10] Y. Chen, H. Liu and G.L. Tao, "Simulation on the port timing of an air-powered engine", *International Journal of Vehicle Design*, no. 38, pp. 259-273, 2005.
- [11] S. Umerujan, T. Gheyret, T. Buso and T. Teruo, "Speed control of general-purpose engine with electronic governor", *Electrical Engineering in Japan*, no. 2, pp. 64-71, 2012.
- [12] Y. Zhang, T. and P.G. Mehta, "Feedforward and feedback adaptive control design and analyses", *Proceedings of 14th IFAC World Congress*, pp. 409-414, 1999.
- [13] Y.H. Tao, "New Type of PID Control and its Application", Beijing: Machinery Industry Press, no. 3, 1998, pp. 286-297.
- [14] B.D. Wood, "Applications of Thermodynamics", Massachusetts: Addison-Wesley Publishing Company, 1982, pp. 286-297.
- [15] R.S. Lu, "Heat Transfer and Thermal Loading in Internal Combustion Engine", Beijing: People's Traffic Press, 1988.
- [16] J.B. Heywood, "Internal Combustion Engine Fundamentals", New York: McGraw-Hill Inc, 1998.
- [17] W. Xu, "The Modern Design Of Automobile Engine", Beijing: People's Traffic Press, 1995.
- [18] S. Menon, N. Moulton and C. Cadou "Development of a dynamometer for measuring small internal-combustion engine performance", *Journal of Propulsion and Power*, no. 23, pp. 194-202, 2007.
- [19] D.Y. Xue and Y.Q. Chen "Technology and Application of System Simulation Based on MATLAB/Simulink", Beijing: Tsinghua University Press, 2002.
- [20] B.Z. Yu, "Digital Signal Processing", Xi'an: Northwestern Polytechnical University Press, 2002.
- [21] L. Liu, X.L. Yu, J.Q. Hu and P.L. Chen, "Air powered engine design based on Pareto Frontier", *Journal of Zhejiang University (Engineering Science)*, no. 43, pp. 123-127, 2009.
- [22] H.X. Wu and S.P. Shen, "Basis of theory and applications on PID control", *Control Engineering of China*, no. 10, pp. 37-42, 2003.
- [23] Y.J. Lei and S.W. Zhang, "Genetic Algorithm Tools and Applications", Xi'an: Xi'an Electronic Science & Technology University Press, 2005.

Received: May 26, 2015

Revised: July 14, 2015

Accepted: August 10, 2015

© Caihong et al.; Licensee Bentham Open.

This is an open access articles licensed under the terms of the Creative Commons Attribution-Non-Commercial 4.0 International Public License (CC BY-NC 4.0) (<https://creativecommons.org/licenses/by-nc/4.0/legalcode>), which permits unrestricted, non-commercial use, distribution and reproduction in any medium, provided that the work is properly cited.